Game-Theoretic Model Predictive Control for Safety-Assured Autonomous Vehicle Overtaking in Mixed-Autonomy Environment

Sheng Yu, Boli Chen, Imad M. Jaimoukha and Simos A. Evangelou

***Abstract*— This work proposes a robust control strategy for an autonomous vehicle to overtake safely and comfortably a human-driven vehicle. The proposed scheme designs a collision-avoidance constraint setup that comprehensively coordinates dimension-based and velocity-dependent constraints to fulfil the safety criteria. A three-phase control framework is proposed for the overtaking task, subject to separate collision-avoidance constraints in lane changing, passing, and merging phases. Moreover, the proposed method utilises a Stackelberg game model to interactively involve the human-driven overtaken vehicle behaviours in the online optimisation loop. To further cope with uncertainties caused by the human driver, the optimisation is solved by a robust model predictive controller to guarantee the avoidance of collisions. Numerical case studies verify that the proposed framework is capable of overtaking not only a cooperative human-driven vehicle but also an uncooperative human-driven vehicle with safe and comfortable trajectories.**

I. INTRODUCTION

With the development of modern autonomous driving techniques, optimal control strategies of connected and autonomous vehicles (CAVs) have been extensively studied [1]. Compared with driving scenarios such as adaptive cruise control [2], and intersection coordination [3], where the majority motions are on the longitudinal direction, the modellings of overtaking problems also study lateral movements of the ego vehicle, with vehicle models varying from an accurate full-size four-wheel model to a simplified bicycle model, seeking a good balance between the model accuracy and complexity [4]. In addition, the setup of the 2-dimensional collision-avoidance constraints is a particular research concern in autonomous overtaking. Specifically, a safety constraint combining ellipse- and rectangle-shapes is proposed in [5] where the ellipse-shaped model involves the heading angle of the obstacle into the constraint expression while the rectangle-shaped model conservatively reserves the safety space. Moreover, [6] aims to ensure that all corner points of the polygon that represents the occupied area of the ego vehicle are always located outside of another polygon that represents the obstacle occupancy. To further make the collision-avoidance constraint more realistic, the work in [7] utilises a phase-based constraint setup which depends on vehicle velocity. However, this setup does not specifically exclude the risk of collisions while the car is steering.

On the other hand, previous overtaking research usually assumes the overtaken vehicle is connected and therefore the movement is known to the ego vehicle [8]. However, this is not realistic when the overtaken vehicle is a human-driven vehicle (HDV). To address the human behaviours that are hard to be formulated explicitly but may significantly affect the controlled loop, [9] proposes a hierarchical learning framework with an offline module trained by historical traffic data and an online module learning from the specific driver to refine the prediction. However, this solution requires extensive learning and training in advance. A novel idea that emerged in the literature is to properly formulate the interaction between the overtaking CAV and the overtaken HDV by utilising game theory, and the Stackelberg game has been shown feasible [10]. A human-like decision-making strategy is presented in [11] to address the co-existence of CAVs and HDVs. During the process of game-based decision making, different human driving styles and interaction behaviours are formulated and considered regarding safety, comfort, and efficiency. Moreover, a robust overtaking scheme is proposed in [12] with a risk-aware reachability analysis that reflects the possible human driver behaviours. However, the involvement of human-caused uncertainties makes it difficult to find feasible solutions for the optimisation problem, unless some assumptions are adopted. To summarise, previous work utilising the Stackelberg game theory usually assumes the human driver performs exactly as the game prediction without considering unpredictable/erratic human behaviours. Although some human uncertainties are addressed in [12] through martingale theory, those exclude driving behaviours such as speeding up that make it difficult to find feasible solutions. Therefore, a further control design which not only considers human behaviours in CAV-HDV interactions but also can provide feasible solutions without being too conservative is missing and is the subject of the present work.

The contribution of the paper is threefold: 1) it designs a practical piece-wise collision-avoidance constraint setup for an overtaking-overtaken vehicle pair that considers vehicle dimensions and velocities; 2) it introduces a new overtaking-overtaken vehicle interactive model based on the concept of Stackelberg game, which further incorporates a stochastic human driver cooperation index that captures the compliance of the human driver to the game solution; 3) the resulting game theoretic problem is solved by a robust model predictive controller (MPC) that accounts for the human driver cooperation uncertainty; numerical case studies validate the effectiveness of the proposed framework in controlling an autonomous vehicle to safely and comfortably complete overtaking of a human-driven vehicle.

The rest of the paper begins in Section II with the introduction of the overtaking problem with an emphasis on the proposed collision-avoidance constraint setup, followed by Section III that explains the vehicle interactions formulated as the Stackelberg game with uncertain human behaviours. Moreover, simulation results are evaluated in Section IV and conclusions are provided with a future plan in Section V.

II. OVERTAKING PROBLEM STATEMENT

This work solves an optimal control problem (OCP) for an overtaking scenario, as illustrated by Fig. 1, where a controlled CAV, denoted as an ego vehicle (EV) is driving at its cruising speed (v_c) and encounters a slow-moving HDV denoted as an obstacle vehicle (OV) ahead. Both vehicles are assumed to be driven in the middle of the initial lane. This work considers the left-hand traffic, where the overtaking

This work has been supported by The Royal Society Grant IES\R2\212041.

S. Yu, I. M. Jaimoukha and S. A. Evangelou are with the Dept. of Electrical and Electronic Engineering at Imperial College London, UK (sheng.yu17@ic.ac.uk, i.jaimouka@ic.ac.uk,s.evangelou@ic.ac.uk).
B. Chen is with the Dept. of Electronic and Electrical Engineering at University College London, UK (boli.chen@ucl.ac.uk)

lane is on the right side of the initial lane. The EV is requested to overtake the OV by crossing the white dashed line, temporarily occupying an overtaking lane, and merging back to the initial lane, with proper control of its steering angle while maintaining its cruising speed v_c during the entire overtaking, which is also known as flying overtaking [13]. The proposed overtaking scheme aims for the EV to avoid collisions with the OV or road boundaries and to maximise its driving comfort during overtaking manoeuvres, with the adoption of the following assumption.

Assumption 1: There are no trailing, leading, or oncoming vehicles on the overtaking lane. The lane width (W_l) is uniform for each lane in the work, and the road remains straight for the whole scenario. The dimensions (lengths and widths) and powertrain limits (acceleration and deceleration) of the EV and OV are identical. Only the front wheels of the EV can be steered. The OV stays in the middle of the initial lane and does not change its lane while being overtaken, thus its displacement perpendicular to the road is zero.

A. Vehicle model

As illustrated by the blue vehicle in Fig. 1, this work utilises a kinematic bicycle model to formulate the motions of the EV during overtaking, where the vehicle side slip angle is neglected ($\beta = 0$ in Fig. 1) and the small angle approximation is adopted for trigonometric quantities, such that this model keeps a reasonable balance between modelling realism and formulation complexity [12], [14], [15].

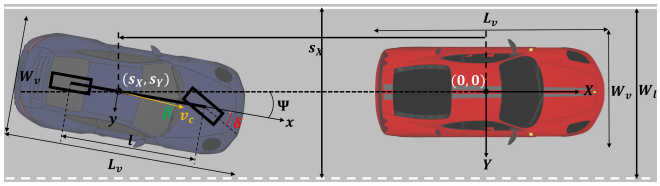

Fig. 1: Illustration of the bicycle model of the EV and relevant parameters in the vehicle overtaking scenario; the red vehicle is the OV. The x- and y-axes attached to the EV denote its longitudinal and lateral directions, respectively.

By defining a moving coordinate system with the origin (0,0) attached to the geometric centre of the OV and X- and Y-axes directions fixed with respect to Earth (road), as shown in Fig. 1, the relative vehicle dynamics of the EV along the road (X-axis) and perpendicular to the road (Y-axis), as well as the rotational dynamics of the EV, can be represented by the following system equations in discrete time subject to a sampling interval $\Delta T \in \mathbb{R}_{>0}$

$$s_X(t+1) = s_X(t) + (v_c - v_{OV}(t))\,\Delta T, \tag{1a}$$
$$s_Y(t+1) = s_Y(t) + v_c \Psi(t) \Delta T, \tag{1b}$$
$$\Psi(t+1) = \Psi(t) + \frac{v_c}{l}\delta(t)\Delta T, \tag{1c}$$

where the sampling index $t \in \mathbb{N}_{[0,t_f]}$ with the total number of samples $t_f = T_f/\Delta T \in \mathbb{N}_{>0}$ (T_f is the predefined total time of overtaking manoeuvre). s_X is the distance of the geometric centre of the EV along the X-axis from the origin attached to the OV, while s_Y is the displacement of the EV geometric centre point along the Y-axis, as the OV stays in the middle of the initial lane while being overtaken. v_c is the constant EV geometric centre velocity with respect to Earth along the x-axis (longitudinal to the EV, see Fig. 1) and $v_{OV}(t)$ is the actual OV velocity with respect to Earth along the X-axis direction. $\Psi(t)$ and $\delta(t)$ denote the EV heading (yaw) angle and front wheel steering angle, respectively. l is the wheelbase length of the EV.

In addition, the state of EV heading angle $\Psi(t)$ and the control input of steering angle $\delta(t)$ are subjected to

$$\underline{\Psi} \le \Psi(t) \le \overline{\Psi}, \quad \underline{\delta} \le \delta(t) \le \overline{\delta}, \tag{2}$$

where $\underline{\Psi}/\overline{\Psi}$ and $\underline{\delta}/\overline{\delta}$ are realistic and small vehicle heading and steering angle bounds during the overtaking, respectively. The sign of $\delta(t)$ indicates the turning direction, with positive for right turning and negative for left turning.

B. Collision-avoidance constraints

In addition to the above heading and steering angle limits of the EV, further coupled constraints for avoiding collisions are also required by the overtaking control strategy. The novel collision-avoidance constraints utilised in this work robustly consider the geometric collision-avoidance constraint between both vehicles, which is illustrated in Fig. 2. As it can be noticed, the occupancy area of a normal passenger vehicle (i.e, EV or OV) can be approximated as a rectangle with length L_v and width W_v (dimensions shown in Fig. 1), which is illustrated by a dashed dark blue rectangle, for example, at the top left box of Fig. 2. This rectangle is further extended to an arc-polygon enclosed by solid dark blue straight line segments and arcs to reserve more gap on each side to cope with extra occupancy in the Y-direction caused by steering and heading angle perturbations during driving and lane changing. The coordinates that define the arc-polygon (i.e., (s_{X_m}, s_{Y_m}), $\forall m \in \{A,B,C,D,E,F\}$) are dependent on the EV geometric centre point coordinates (s_X, s_Y), the length of vehicle diagonal (diagonal of the dashed rectangle, $2r = \sqrt{L_v^2 + W_v^2}$), the angle between the diagonal and long side of the dashed rectangle (θ), and the maximum heading angle ($\overline{\Psi}$) of the EV.

Moreover, based on this vehicle dimension-based setup, the velocity-dependent collision-avoidance constraints are implemented, which are illustrated by light blue, green, and purple piece-wise segments in Fig. 2 connecting points $(s_{X_n}, s_{Y_n}, \forall n \in \{a,b,c,d,e\})$. Points (s_{X_a}, s_{Y_a}) and $(s_{X_e}(t), s_{Y_e})$, where $s_{X_a} = -(d_{X0} + v_c t_0)$ and $s_{X_e}(t) = d_{X0} + v_{OV}(t)(t_r + t_0)$, define the minimum X-direction safe gap between the geometric centres of the two vehicles when they are both in the middle of the initial lane ($s_{Y_a} = s_{Y_e} = 0$) before and after the overtaking, respectively. $d_{X0} = s_0 + 2r$ represents a velocity-independent term including the standstill headway gap (s_0) as well as the vehicle diagonal length ($2r$), t_0 is the minimum time gap in car-following, and t_r is the response time of the human driver of the OV. As the EV changes to or merges from the overtaking lane ($s_Y(t) > 0$), it is allowed to be $s_{X_a} < s_X(t) < s_{X_e}(t)$ after the overtaking starts and before it finishes, while the Euclidean distance between the two vehicle geometric centres should satisfy $\sqrt{s_X(t)^2 + s_Y(t)^2} \ge 2r$ to ensure the avoidance of collision, which is illustrated by the dashed red circle in Fig. 2. Note that the latter condition is desirable when both the EV and OV undergo large heading angle changes, which, however, is not the case in the present work. Therefore, this condition can be too conservative, particularly from the Y-direction perspective (i.e., blocking the entire overtaking lane) and impractical in real traffic. After practically setting the heading angle limits of EV and OV ($\overline{\Psi}$ and $\overline{\Psi}_{OV}$), the minimum safe gap when the EV is passing on the side of the OV is relaxed from $2r$ to $s_{Y_c} = r\sin(\theta + \overline{\Psi}) + r\sin(\theta + \overline{\Psi}_{OV})$. This defines the green segment passing through the point (s_{X_c}, s_{Y_c}) in Fig. 2 at constant offset s_{Y_c} from the Y-axis, along which this gap condition applies. Furthermore, the green segment intercepts

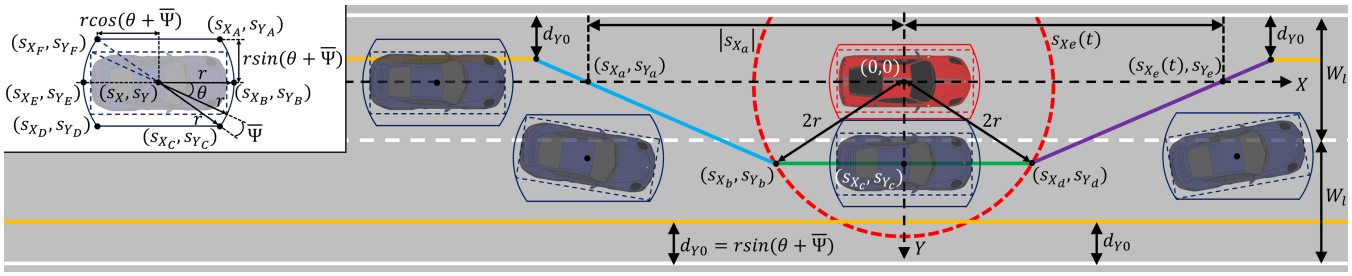

Fig. 2: A three-phase-based collision-avoidance constraint setup. The OV is centred at the origin (0,0) of an X-Y coordinate system. The blue vehicles illustrate possible occupancies of the EV during the overtaking, centred at position (s_X, s_Y). Note that the associated dark blue arc-polygon around the EV is wider than the associated red arc-polygon around the OV, where the arc-polygons capture the range of heading angle changes in each vehicle. Road boundaries and road lane markings are denoted by solid and dashed white lines, respectively.

the dashed red circle at points (s_{X_b}, s_{Y_b}) and (s_{X_d}, s_{Y_d}), which define the margins of the green segment. Note that along the green segment, the arc-polygons of the EV and OV merely touch but do not overlap.

By connecting points (s_{X_a}, s_{Y_a}) with (s_{X_b}, s_{Y_b}) and (s_{X_d}, s_{Y_d}) with (s_{X_e}, s_{Y_e}) accordingly, collision-avoidance constraints for the periods of changing lane and merging back are obtained and illustrated by the light blue and purple segments in Fig. 2. Moreover, to avoid collision with roadside barriers, the centre point of the EV should always maintain a minimum Y-direction distance (d_{Y0}) to roadsides, as visualised by yellow segments in Fig. 2. Hence, to fulfil the collision-avoidance requirement, the centre point of the EV should remain within the area bounded by light blue, green, purple, and yellow segments during overtaking. These marginal collision-avoidance constraints are mathematically represented as

$$\frac{s_{Y_b}-s_{Y_a}}{s_{X_b}-s_{X_a}} s_X(t) + \left(s_{Y_a} - \frac{s_{X_a}(s_{Y_b}-s_{Y_a})}{s_{X_b}-s_{X_a}} \right) \leq s_Y(t), \forall s_X(t) \leq s_{X_b}, \quad \text{(3a)}$$

$$s_{Y_c} \leq s_Y(t), \qquad \forall s_{X_b} < s_X(t) \leq s_{X_d}, \quad \text{(3b)}$$

$$\frac{s_{Y_e}-s_{Y_d}}{s_{X_e}(t)-s_{X_d}} s_X(t) + \left(s_{Y_d} - \frac{s_{X_d}(s_{Y_e}-s_{Y_d})}{s_{X_e}(t)-s_{X_d}} \right) \leq s_Y(t), \forall s_{X_d} < s_X(t), \quad \text{(3c)}$$

$$-\frac{1}{2}W_l + d_{Y0} \leq s_Y(t) \leq \frac{3}{2}W_l - d_{Y0}, \quad \forall s_X(t) \in \mathbb{R}, \quad \text{(3d)}$$

inferred from the light blue, green, purple, and yellow boundaries, respectively.

C. Control framework and objectives

In line with the three (light blue, green, purple) segments defined in Section II-B, a three-phase MPC algorithm is proposed for the overtaking task, subject to state equations (1), independent constraints (2), common collision-avoidance constraint (3d), and a separate collision-avoidance constraint from (3a)-(3c). For the sake of further discussion, let us denote the phases with constraints represented by the light blue, green, and purple segments as lane changing phase, passing phase, and merging phase, respectively. The EV executes lane changing, passing, and merging manoeuvres during overtaking in turns, according to the status of $s_X(t)$.

This work shows that the overall overtaking OCP can be addressed by three cascaded finite-horizon optimal control problems (FHOCPs). In addition to satisfying the constraints introduced above, each FHOCP aims to optimise its own objective function containing common (across all FHOCPs) and separate objective terms, collectively emphasising the same targets on comfort and safety during the manoeuvre. Similar to the common approach in the literature [16], comfort during overtaking can be quantitatively evaluated by investigating solely the EV Y-direction acceleration ($a_Y(t) \approx \frac{v_c^2}{l}\delta(t)$) which is proportional to $\delta(t)$. As such, it is reasonable to penalise the L^2-norm of $\delta(t)$ for enhanced comfort. Meanwhile, to reduce the heading oscillations, $\Psi(t)$ can be penalised similarly, leading to two individual stage costs

$$J_c^{(p)} = \sum_{k=0}^{N-1} \delta(t+k|t)^2, \quad J_h^{(p)} = \sum_{k=0}^{N-1} \Psi(t+k|t)^2. \quad \text{(4)}$$

where the superscript $p \in \{1,2,3\}$ indicates lane changing, passing, and merging phases, respectively. $k \in \mathbb{N}_{[0,N-1]}$ is the step index of a prediction horizon with length N.

On the other hand, although the collision-avoidance constraints specified in (3) provide a theoretical baseline guarantee of safety, the solutions will be less prone to infeasibilities if the movement of the EV could follow a target trajectory away from constraints. Therefore, three safety-concerned objective functions are designed for the three phases regarding each collision-avoidance constraint ((3a)-(3c)), respectively

$$J_s^{(1)} = \left(s_Y(t+N|t) - W_l\right)^2, \quad \text{(5a)}$$

$$J_s^{(2)} = \sum_{k=0}^{N-1} \left(s_Y(t+k|t) - W_l\right)^2, \quad \text{(5b)}$$

$$J_s^{(3)} = \sum_{k=0}^{N-1} \left(s_Y(t+k|t) - 0\right)^2. \quad \text{(5c)}$$

Specifically, (5a) contains a terminal cost such that the EV aims to reach the middle of the overtaking lane which is also the target position of the entire passing phase as claimed in (5b). Hence, a smooth and continuous trajectory is expected as the EV propagates from the lane changing phase to the passing phase. Furthermore, (5c) pushes the EV to merge back to the middle of the original lane in the merging phase. Therefore, the control framework of the lane-changing and passing phases, where interactions between the two vehicles are not triggered yet, can be formulated as FHOCP 1 and FHOCP 2, respectively, as

FHOCP 1 (if $s_X(t) \leq s_{X_b}$):

$$\min_{\delta(t+k|t)} \quad J_1 = W_c^{(1)} J_c^{(1)} + W_h^{(1)} J_h^{(1)} + W_s^{(1)} J_s^{(1)} \quad \text{(6a)}$$

$$s.t. \quad s_X(t+k+1|t) = s_X(t+k|t) + (v_c - v_{OV}^*(t+k|t) + w_{12}(t+k|t))\Delta T, \; k \in \mathbb{N}_{[0,N-1]} \quad \text{(6b)}$$

$$\underline{w}_{12} \leq w_{12}(t+k|t) \leq \overline{w}_{12}, \quad \text{(6c)}$$

(1b), (1c), (2), (3a), (3d), (4), (5a).

FHOCP 2 (if $s_{X_b} < s_X(t) \leq s_{X_d}$):

$$\min_{\delta(t+k|t)} \quad J_2 = W_c^{(2)} J_c^{(2)} + W_h^{(2)} J_h^{(2)} + W_s^{(2)} J_s^{(2)}, \tag{7a}$$

$$s.t. \quad (1b),(1c),(2),(3b),(3d),(4),(5b),(6b),(6c)$$

where $W_c^{(1)}$, $W_h^{(1)}$, $W_s^{(1)}$, $W_c^{(2)}$, $W_h^{(2)}$, and $W_s^{(2)}$ are weighting parameters of each associated objective term. The exogenous input $v_{OV}^*(t)$ is the predicted velocity of the OV, which is assumed to be a constant velocity within the prediction horizons of FHOCP 1 and FHOCP 2, following a common approach [17]. $w_{12}(t) \in [\underline{w}_{12}, \overline{w}_{12}]$ is the mismatch between the real and predicted OV velocities, subject to its associated boundaries. The FHOCP of the merging phase depending on the interactions between the two vehicles will be addressed in the next section by a game-based control strategy.

III. Interactions between vehicles

This section models interactions between the controlled EV and the human-driven OV as a Stackelberg game [11] with a novel human driver cooperation index to reflect the uncertain cooperative intentions of the overtaken human driver. Unlike other Nash equilibrium based algorithms where decisions are made independently, the Stackelberg game based algorithm considers the other player behaviours and hence makes decisions accordingly, which emphasises the interaction between the EV and OV. This work assumes that interactions between the two vehicles are not triggered until the EV enters the merging phase (i.e., $s_{X_d} < s_X(t)$), where the OV not only maximises its own driving satisfaction, but also responds to behaviours of the EV.

A. Stackelberg game model

According to the Stackelberg game model, the interaction between two vehicles is formulated as two cascaded FHOCPs for two players (i.e., the sub-game for the leader, EV, and sub-game for the follower, OV), respectively. The purpose of solving the OV sub-game is to determine the optimal solution of the OV given all possible actions of the EV. Moreover, the determined optimal solution of the OV is involved in the EV sub-game as an exogenous input which will ultimately affect the optimal solution of the EV sub-game. Inspired by previous literature on driver modelling, especially in car-following scenarios [18], [19], the OV sub-game is formulated as FHOCP 3 as

FHOCP 3 (if $s_{X_d} < s_X(t)$):

$$\begin{aligned} \min_{\substack{u_{OV}(t+k|t) \\ \delta(t+k|t)}} \quad J_{OV} = \sum_{k=0}^{N-1} \Big(& W_{OV1}(u_{OV}(t+k|t)-0)^2 + \\ & W_{OV2}\Big(v_{OV}(t+k|t) - v_{OV,i}^{(3)}\Big)^2 + \\ & W_{OV3}(s_X(t+k|t) - \bar{s}_X(t+k|t))^2 \Big), \end{aligned} \tag{8a}$$

$$s.t. \quad v_{OV}(t+k+1|t) = v_{OV}(t+k|t) + u_{OV}(t+k|t)\Delta T, \tag{8b}$$

$$0 \leq v_{OV}(t+k|t) \leq \bar{v}, \quad k \in \mathbb{N}_{[0,N-1]} \tag{8c}$$

$$\underline{u} \leq u_{OV}(t+k|t) \leq \overline{u}, \tag{8d}$$

$$(1),(2),(3c),(3d),$$

where W_{OV1}, W_{OV2}, and W_{OV3} are weighting parameters addressing comfort, velocity, and following gap objectives of the OV. Moreover, $v_{OV,i}^{(3)}$ is the initial OV velocity when the EV enters the merging phase, which is also reasonably deemed as the desired OV velocity while being overtaken. The OV velocity determined by (8b) satisfies (8c), where $u_{OV}(t)$ is the acceleration of the OV, subject to common vehicle physical limits as shown in (8d) [20]. $\bar{s}_X(t) = d_{X0} + v_{OV}(t)t^*$ is the velocity-dependent desired following distance given a desired car-following time gap t^*. The objective of maintaining a desired relative distance gap requires cooperative OV responses (i.e., slow down to yield) if $s_X(t) < \bar{s}_X(t)$. Furthermore, FHOCP 3 is also subject to other constraints applied to the EV during the merging phase ((2), (3c),(3d)), such that all possible actions of the EV are involved in FHOCP 3. Let us denote $u_{OV}^*(t)$ as the game-determined optimal solution of FHOCP 3 given all possible actions of the EV. Hence the predicted OV velocity ($v_{OV}^*(t)$) can be obtained by substituting $u_{OV}^*(t)$ for $u_{OV}(t)$ in (8b). Note that the optimal solution $u_{OV}^*(t)$ determined by FHOCP 3 not only aims to maximise human driver own satisfaction while being overtaken [19], but also is a cooperative driving response because of minimising the third objective term in (8a). Therefore, the human driver is regarded as cooperative if the actual behaviour is aligned with $u_{OV}^*(t)$.

Based on the optimal solution $u_{OV}^*(t)$ of the OV sub-game (FHOCP 3), the EV sub-game can be formulated as follows

FHOCP 4 (if $s_{X_d} < s_X(t)$):

$$\min_{\delta(t+k|t)} \quad J_3 = W_c^{(3)} J_c^{(3)} + W_h^{(3)} J_h^{(3)} + W_s^{(3)} J_s^{(3)}, \; k \in \mathbb{N}_{[0,N-1]} \tag{9a}$$

$$s.t. \quad v_{OV}^*(t+k+1|t) = v_{OV}^*(t+k|t) + u_{OV}^*(t+k|t)\Delta T, \tag{9b}$$

$$s_X(t+k+1|t) = s_X(t+k|t) + (v_c - v_{OV}^*(t+k|t))\Delta T, \tag{9c}$$

$$(1b),(1c),(2),(3c),(3d),(4),(5c),$$

where $W_c^{(3)}$, $W_h^{(3)}$, and $W_s^{(3)}$ are associated weights of objectives. The predicted OV velocity $v_{OV}^*(t)$ is determined based on the optimal solution ($u_{OV}^*(t)$) provided by FHOCP 3.

B. Human driver cooperation index

Although the current algorithm has already involved game-based competitive interactions between the connected EV and the human-driven OV, the formulation is still idealised as the EV assumes the OV velocities can be accurately predicted by the game model, as in (9b). In reality, the human driver may perform as the game predicts, or may not respond, or behave with contrasting actions. To cope with this human-caused uncertainty, we define a parameter called the human driver cooperation index (HDCI), denoted as $\eta(t)$, such that the connection between the actual human driver behaviours ($u_{OV}(t)$) with the game-based predictions ($u_{OV}^*(t)$) is expressed as $u_{OV}(t) = \eta(t) u_{OV}^*(t)$ with $\eta(t) \in [-1, 1]$. Specifically, the sign and magnitudes of $\eta(t)$ indicate how cooperative is the human driver response, e.g., $\eta(t) = 1$, $\eta(t) = 0$, and $\eta(t) = -1$ represent full cooperative, no response, and full uncooperative, respectively. This work assumes that $\eta(t)$ is a Gaussian distributed random number, $\eta(t) \sim \mathcal{N}(\mu, \sigma^2)$. The mean of the Gaussian distribution is zero, $\mu = 0$. The variance of the Gaussian distribution (σ^2) is a function of the perception of the human driver of the X-direction time gap ($\Delta t_X(t) = \frac{s_X(t)}{v_{OV}(t)}$) such that σ converges to zero as $\Delta t_X(t)$ increases. This is understood as the EV moves further ahead after passing the OV, the human driver is less likely to respond to the overtaking vehicle [21], [22]. A qualitatively compatible example illustration of the bivariate probability density function (PDF) of the HDCI is visualised in a 3D map in Fig. 3, while a quantitatively accurate PDF of the HDCI can be determined after analysing a large-size human driver dataset, which is beyond the scope of the present work. By considering such uncertain human behaviours, a more realistic expression of $v_{OV}^*(t)$ is represented as

$$v_{OV}^*(t+1) = v_{OV}^*(t) + (u_{OV}^*(t) + w_3(t))\Delta T, \tag{10}$$

where the additive disturbance $w_3(t) = (\eta(t)-1)u^*_{OV}(t)$. Since $\eta(t)$ has a Gaussian distribution and its variance converges to zero as $\Delta t_X(t)$ increases, a parameter denoted as $\eta^* \in \mathbb{R}_{\geq 0}$ is introduced such that the η^* confidence interval boundaries are adopted as the boundaries of $\eta(t)$ rather than $[-1,1]$ to reduce the tightness of disturbance boundaries. The upper and lower confidence interval boundaries are denoted as $\overline{\eta}_{\eta^*}(t)$ and $\underline{\eta}_{\eta^*}(t)$ ($\underline{\eta}_{\eta^*}(t) = -\overline{\eta}_{\eta^*}(t)$), respectively.

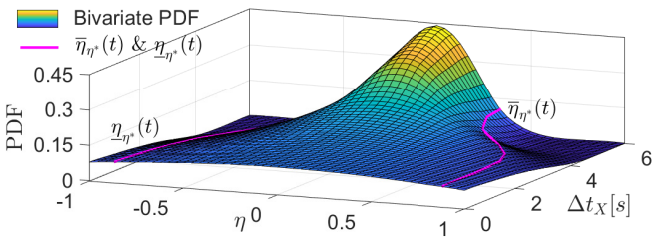

Fig. 3: An example illustration of the bivariate probability density function (PDF) of $\eta(t)$ at various $\Delta t_X(t)$. $\eta(t)$ is normalised between -1 and 1. $\Delta t_X(t)$ varies from zero up to the time gap, where the PDF is truncated. Pink curves represent an example of $\eta^*=95\%$ confidence interval boundaries ($\overline{\eta}_{\eta^*}(t)$ and $\underline{\eta}_{\eta^*}(t)$).

Thus, the disturbance-free FHOCP 4 is replaced by a realistic FHOCP

FHOCP 5 (if $s_{X_d} < s_X(t)$):

$$\min_{\delta(t+k|t)} \quad \text{(9a)},$$
$$s.t. \quad \underline{w}_3(t+k|t) \leq w_3(t+k|t) \leq \overline{w}_3(t+k|t), \quad \text{(11a)}$$
$$\text{(1b)},\text{(1c)},\text{(2)},\text{(3c)},\text{(3d)},\text{(4)},\text{(5c)},\text{(9c)},\text{(10)},$$

where $\underline{w}_3(t+k|t) = \min\{-(1+\overline{\eta}_{\eta^*}(t+k|t))u^*_{OV}(t+k|t), (\overline{\eta}_{\eta^*}(t+k|t)-1)u^*_{OV}(t+k|t)\}$ and $\overline{w}_3(t+k|t) = \max\{(\overline{\eta}_{\eta^*}(t+k|t)-1)u^*_{OV}(t+k|t), -(1+\overline{\eta}_{\eta^*}(t+k|t))u^*_{OV}(t+k|t)\}$ such that the disturbance boundaries in (11a) are dependent on the game-based prediction $u^*_{OV}(t+k|t)$ to reduce conservativeness. Note that the only difference between FHOCP 4 and FHOCP 5 is the replacement of the disturbance-free expression (9b) by a realistic expression (10) with an additive disturbance subject to the associated constraint (11a).

To sum up, the three-phase finite-horizon controller formulated as FHOCP 1, FHOCP 2, and FHOCP 5 are solved by a recently proposed robust MPC [20], respectively. FHOCP 3 of the OV sub-game is solved by a nominal MPC.

Remark 1: Since the EV longitudinal velocity is constant at v_c in the present work, in cases where the OV speeds up (aggressively prevents the EV from cutting in) such that safely overtaking is no longer feasible, an emergency handling rule can be triggered to force the EV to remain in the overtaking lane.

IV. Simulation Results

The performance of the proposed method is assessed twofold: 1) the weights of the objective function are tuned through trial and error such that the controller can reach a balance between the two targets on safety and comfort; 2) the proposed overtaking strategy is tested by using two OV profiles to demonstrate its capability of handling cooperative and uncooperative human driver behaviours. All simulation examples are solved by the Yalmip toolkit with the MOSEK solver in the Matlab environment. The sampling interval of the controller is set at $\Delta T = 0.1$ s and the prediction horizon length is chosen as $N = 10$ steps such that the prediction horizon covers the length of the minimum time gap (t_0) between two vehicles. The main characteristic parameters of the overtaking problem are summarised in Table. I.

TABLE I: Parameters of Overtaking Problem.

Descriptions	Symbols	Values
EV cruising speed/OV speed limit	$v_c/\overline{v}$	22.22/22.22 m/s
Length of half diagonal of vehicle rectangle	r	2.38 m
Angle between vehicle diagonal and long side	θ	22.47°
Length/width/wheelbase of vehicle	$L_v/W_v/l$	4.4/1.82/2.5 m
Width of one lane	W_l	3.65 m
Standstill front-rear distance gap	s_0	2 m
Maximum deceleration/acceleration of vehicle	$\underline{u}/\overline{u}$	-3.5/3.5 m/s^2
Minimum/desired time gap	t_0/t^*	1/2 s
Driver response time	t_r	0.7 s

The safety-related performance is quantitatively evaluated by the cut-in distance (s^*_X) which is defined as the relative X-direction distance between two vehicles when the EV mergers back to the initial lane, i.e., $s^*_X = s_X(t)$ when $s_Y(t) = \frac{W_l}{2} - d_{Y0}$. A large s^*_X suggests the EV occupies the overtaking lane for a long distance, which might unnecessarily affect other traffic. On the other hand, the comfort level is evaluated by the root mean squared (RMS) acceleration in the Y-direction, $a_{Y,RMS} = \sqrt{\frac{1}{k_{s3}}\sum_{i=0}^{k_{s3}-1} a_Y(i)^2}$, where k_{s3} is the number of samples in the merging phase. Therefore, the objectives of safety and comfort are in conflict, as achieving a small cut-in distance might result in a large acceleration value. Hence, an exhaustive search is performed to find the optimal weighting parameters $W_c^{(3)}$, $W_h^{(3)}$, and $W_s^{(3)}$ at the nominal cooperative situation ($w_3(t) = 0$) that offer a decent compromise between minimisation of s^*_X and $a_{Y,RMS}$, with 15 different values searched for each weight, i.e. a total of $15^3 = 3375$ combinations. Once the optimal weights are found, each one is further swept in turn around its optimal value to provide an exemplary illustration of its influence on the performance objectives, as a Pareto type analysis, as shown in Fig 4. In these results, the cut-in distance varies from 15 m to 104 m while the $a_{Y,RMS}$ varies from 0.03 m/s^2 to 1.56 m/s^2, and with the optimal weighting parameters the two conflicting objectives reach a balance with 72% of the most individual performance for both criteria.

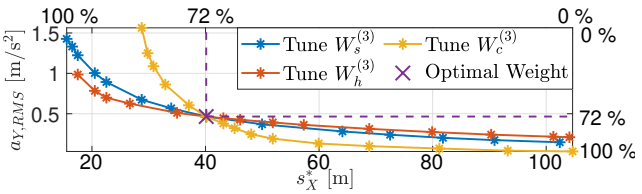

Fig. 4: Optimal weighting parameter choices of FHOCP 5 in the merging phase, achieving a decent compromise in the performance of both objectives.

Based on the optimised weights, further case studies are performed to verify the capability of the proposed scheme in dealing with two different human-driven OV responses in Fig. 5. When the OV cooperates by slowing down to yield, the EV successfully overtakes the OV with a safe trajectory (see Fig. 5a). In the case of an uncooperative OV driver, although the OV speeds up when the EV is attempting to merge back, the EV still manages to return to the original lane by adjusting $\delta(t)$ to create space for the accelerating OV. This ensures that the collision-avoidance requirements mentioned earlier are satisfied as the OV approaches from

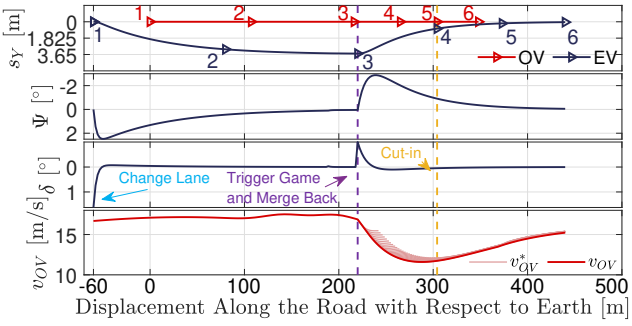

(a) A case when OV is cooperative ($\eta(t) = \overline{\eta}_{95\%}(t)$).

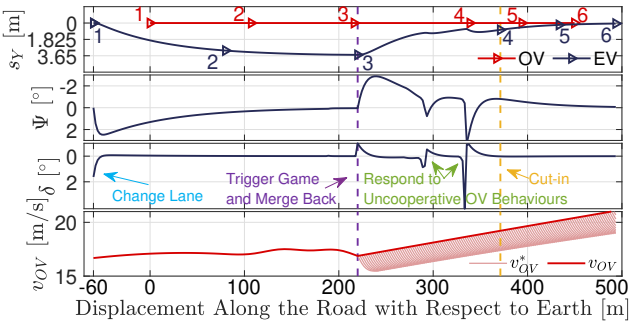

(b) A case when OV is uncooperative ($\eta(t) = 0.1\underline{\eta}_{95\%}(t)$).

Fig. 5: Profiles of EV overtaking trajectory and OV velocity for different case studies (i.e., $\eta(t) = \overline{\eta}_{95\%}(t)$ and $\eta(t) = 0.1\underline{\eta}_{95\%}(t)$). Blue and red curves represent profiles of OV and EV, respectively. The purple dashed lines denote when the Stackelberg game competitions are triggered in optimisations. The yellow dashed lines denote when the EV cuts in ahead of the OV (i.e., $s_Y(t) = \frac{W_l}{2} - d_{Y0}$), indicating the success of overtaking. In the top subplots of each figure, the positions of EV and OV are marked by numbered triangles indicating the trajectory sequences. EV heading and steering angle profiles are shown in the second and third subplots. The bottom subplot compares the game-based cooperative v^*_{OV} (of each receding horizon) and the actual v_{OV} profiles. Furthermore, (b) illustrates the ability of the proposed overtaking control scheme to deal with an uncooperative OV through effective responses in terms of steering angle adjustments to ensure the compliance of collision-avoidance constraints.

behind. The associated trajectories of the EV and OV are shown in Fig. 5b. Additionally, the profiles of $\Psi(t)$ and $\delta(t)$ confirm the validity of the small angle approximation.

V. Conclusions and Future Work

This work addresses an autonomous overtaking control problem while considering the uncertain behaviours of the overtaken vehicle human driver. To guarantee safety during overtaking manoeuvres, a robust collision-avoidance constraint setup is designed which considers both vehicle dimensions and real-time velocity. Moreover, the proposed scheme uses a Stackelberg game-based framework to predict future behaviours of the overtaken vehicle and set up disturbance boundaries to cope with human-caused uncertainties. By tuning the weights of the objective function, the presented control framework is able to keep a balance between safety and comfort during overtaking. Numerical case studies illustrate that the proposed overtaking strategy is capable of overtaking both cooperative and uncooperative human-driven overtaken vehicles. Future research of this work will emphasise involving a longitudinal velocity control in the control strategy with a realistic human driver cooperation model extracted from realistic datasets.

References

[1] D. González, J. Pérez, V. Milanés, and F. Nashashibi, "A review of motion planning techniques for automated vehicles," *IEEE Transactions on Intelligent Transportation Systems*, vol. 17, no. 4, pp. 1135–1145, 2016.

[2] V. Milanés, S. E. Shladover, J. Spring, C. Nowakowski, H. Kawazoe, and M. Nakamura, "Cooperative adaptive cruise control in real traffic situations," *IEEE Transactions on Intelligent Transportation Systems*, vol. 15, no. 1, pp. 296–305, 2014.

[3] X. Pan, B. Chen, L. Dai, S. Timotheou, and S. A. Evangelou, "A hierarchical robust control strategy for decentralized signal-free intersection management," *IEEE Transactions on Control Systems Technology*, vol. 31, no. 5, pp. 2011–2026, 2023.

[4] S. Dixit, S. Fallah, U. Montanaro, M. Dianati, A. Stevens, F. Mccullough, and A. Mouzakitis, "Trajectory planning and tracking for autonomous overtaking: State-of-the-art and future prospects," *Annual Reviews in Control*, vol. 45, pp. 76–86, 2018.

[5] H. Ren, S. Chen, L. Yang, and Y. Zhao, "Optimal path planning and speed control integration strategy for UGVs in static and dynamic environments," *IEEE Transactions on Vehicular Technology*, vol. 69, no. 10, pp. 10 619–10 629, 2020.

[6] R. Chai, A. Tsourdos, S. Chai, Y. Xia, A. Savvaris, and C. L. P. Chen, "Multiphase overtaking maneuver planning for autonomous ground vehicles via a desensitized trajectory optimization approach," *IEEE Transactions on Industrial Informatics*, vol. 19, no. 1, pp. 74–87, 2023.

[7] S. Jeon, K. Lee, and D. Kum, "Overtaking decision and trajectory planning in highway via hierarchical architecture of conditional state machine and chance constrained model predictive control," *Robotics and Autonomous Systems*, vol. 151, p. 104014, 2022.

[8] Y. Chen, C. Lu, and W. Chu, "A cooperative driving strategy based on velocity prediction for connected vehicles with robust path-following control," *IEEE Internet of Things Journal*, vol. 7, no. 5, pp. 3822–3832, 2020.

[9] C. Lu, H. Wang, C. Lv, J. Gong, J. Xi, and D. Cao, "Learning driver-specific behavior for overtaking: A combined learning framework," *IEEE Transactions on Vehicular Technology*, vol. 67, no. 8, pp. 6788–6802, 2018.

[10] C. Burger, J. Fischer, F. Bieder, Ö. Ş. Taş, and C. Stiller, "Interaction-aware game-theoretic motion planning for automated vehicles using Bi-level optimization," in *2022 IEEE 25th International Conference on Intelligent Transportation Systems (ITSC)*, 2022, pp. 3978–3985.

[11] P. Hang, C. Lv, Y. Xing, C. Huang, and Z. Hu, "Human-like decision making for autonomous driving: A noncooperative game theoretic approach," *IEEE Transactions on Intelligent Transportation Systems*, vol. 22, no. 4, pp. 2076–2087, 2021.

[12] Y. Gao, F. J. Jiang, L. Xie, and K. H. Johansson, "Risk-aware optimal control for automated overtaking with safety guarantees," *IEEE Transactions on Control Systems Technology*, vol. 30, no. 4, pp. 1460–1472, 2022.

[13] G. Asaithambi and G. Shravani, "Overtaking behaviour of vehicles on undivided roads in non-lane based mixed traffic conditions," *Journal of Traffic and Transportation Engineering (English Edition)*, vol. 4, no. 3, pp. 252–261, 2017.

[14] R. Rajamani, *Vehicle dynamics and control*, 2nd ed., ser. Mechanical engineering series. New York: Springer, 2012.

[15] W. F. Milliken and D. L. Milliken, *Race car vehicle dynamics*. Warrendale, PA: Society of Automotive Engineers, Inc., 1995 - 1995.

[16] K. N. de Winkel, T. Irmak, R. Happee, and B. Shyrokau, "Standards for passenger comfort in automated vehicles: Acceleration and jerk," *Applied Ergonomics*, vol. 106, p. 103881, 2023.

[17] G. Guo, Z. Zhao, and R. Zhang, "Distributed trajectory optimization and fixed-time tracking control of a group of connected vehicles," *IEEE Transactions on Vehicular Technology*, vol. 72, no. 2, pp. 1478–1487, 2023.

[18] M. Treiber, A. Hennecke, and D. Helbing, "Congested traffic states in empirical observations and microscopic simulations," *Phys. Rev. E*, vol. 62, pp. 1805–1824, Aug 2000.

[19] J. Fleming, X. Yan, and R. Lot, "Incorporating driver preferences into eco-driving assistance systems using optimal control," *IEEE Transactions on Intelligent Transportation Systems*, vol. 22, no. 5, pp. 2913–2922, 2021.

[20] S. Yu, X. Pan, A. Georgiou, B. Chen, I. M. Jaimoukha, and S. A. Evangelou, "A real-time robust ecological-adaptive cruise control strategy for battery electric vehicles," 2023.

[21] Y. Li, S. Zhang, Y. Pan, B. Zhou, and Y. Peng, "Exploring the stability and capacity characteristics of mixed traffic flow with autonomous and human-driven vehicles considering aggressive driving," *Journal of Advanced Transportation*, 2023.

[22] X. Huang, S. Zhang, and H. Peng, "Developing robot driver etiquette based on naturalistic human driving behavior," *IEEE Transactions on Intelligent Transportation Systems*, vol. 21, no. 4, pp. 1393–1403, 2020.